Meshfree modeling of heat transfer in selective laser melting process

Songtao Chen*, †Qinglin Duan, Shuhui Li, Xikui Li and Hongwu Zhang

The State key Laboratory of Structural Analysis for Industrial Equipment, Department of Engineering Mechanics, Dalian University of Technology, Dalian, Liaoning 116024, P.R.China.

*Presenting author: chensongtao1221@163.com
†Corresponding author: qinglinduan@dlut.edu.cn

Abstract

Selective laser melting (SLM) process produces 'near net shape' parts from a stream of metal powders in a layer-by-layer manner for use in medical, aerospace and other industries. The thermal history generated by SLM is significant in determining the microstructure, mechanical properties, residual stress, and distortion of manufactured components. This study employs three-dimensional element-free Galerkin (EFG) method to investigate the temperature evolution in SLM. The moving heat source and the dependence of material properties on temperature are considered. It is found that the developed meshfree method is able to capture the high gradients of temperature in heat affected zoon. The effects of scan speed and laser power are also investigated.

Keywords: Meshfree; Selective laser melting; Additive manufacturing; EFG; Heat transfer

1. Introduction

Selective laser melting (SLM) is a promising additive manufacturing (AM) technique in which successive layers of metal powders are heated via laser in order to build a part. It has advantages for direct fabrication of three-dimensional (3D) parts with complex structures [1][2]. A typical process of layer by layer SLM fabrication is showed in Figure 1:

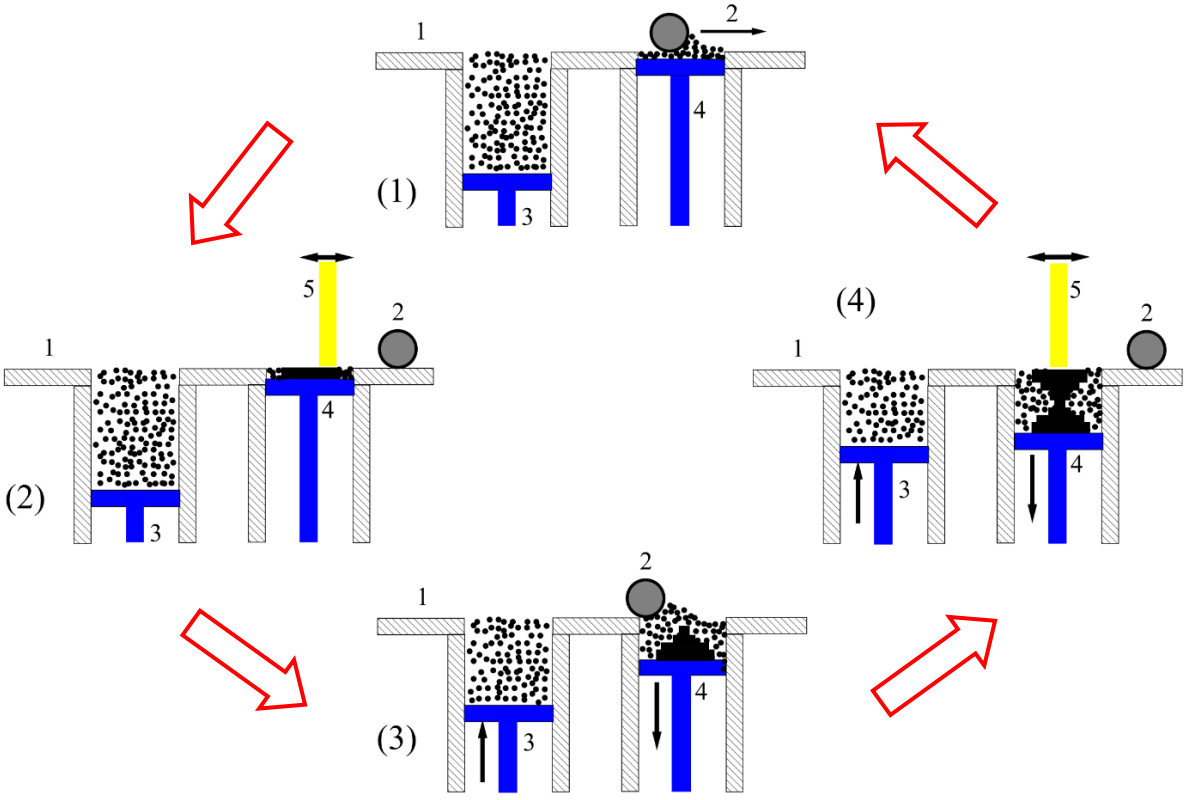

Figure 1.Scheme of the process (1) deposition of a powder layer, (2) scanning of the first layer, (3) deposition of a powder layer in the interval, (4) scanning of the last layer, and preparing for next part.

The SLM machine is composed of a fabrication plate 1 with two holes to which two containers are attached. A roller 2 drives powder from the left container and deposits a thin powder layer in the right container. The thickness of the layer is controlled by pistons moving up 3 and down 4. Then a laser beam 5 scans on the deposited powder under inert-gas protection. The absorbed laser energy melts the powder and makes a molten pool locally. As the molten pool freezes, this part will be fixed on the substrate. The product will be fabricated by repeating this procedure layer-by-layer. After that, the product will be cooled and removed out.

All the manufacturing course of SLM is in an inert-gas protection system, which prevents metal powders from assimilating oxygen, nitrogen, and hydrogen from the atmosphere. But as SLM is a complex physic metallurgy process, the structure always has uncontrollable defects such as balling, distortion, and heat fatigue cracking. Therefore, it is significant to study the thermal behavior during SLM. However, experimental measurements of the temperature during SLM are considered to be almost impossible because of the localized heating and superfast melting and solidification involved. Numerical simulation is a useful measure to solve these problems.

Recently, many FEM models have been established to investigate thermal behavior during AM. Gusarov *et al* [3]-[5] numerically analyzed the temperature distribution of a 316L powder bed during SLM. They discovered that the stability of the process is highly dependent on the scan speed, powder layer thickness, and the thermal properties of the materials. Li [6] studied the scan speed and the power's influence on the size of molten pool, and carried out many experiments of SLM process under different laser processing conditions to demonstrate the reliability of the physical model and simulation results. Hussein *et al* [7] used ANSYS parametric design language (APDL) to develop a non-linear transient model based on sequentially coupled thermo-mechanical field analysis code and simulated the temperature and stress fields in single 316L stainless steel layers built on the powder bed without support in SLM. They found that the predicted length of the molten pool increases at higher scan speed while both width and depth of the melt pool decrease. The cyclic melting and cooling rates in the scanned tracks result in high VonMises stresses in the consolidated tracks of the layer.

Considering that the temperature gradient around the molten pool is very high and fluctuates violently, traditional FEM shape function is difficult to simulate accurately. The meshfree methods [8]-[13] that have the apparent advantage of building highly smooth field is more suitable for this process. Meshfree methods such as the element-free Galerkin (EFG) method developed in recent twenty years have become a formidable competitor to the traditional finite element method (FEM) which dominates engineering analysis for decades. But the basis functions in Galerkin-based meshfree method are rational (nonpolynomial) functions. This is the central issue that introduce numerical errors when using standard Gauss quadrature for numerical integration. The errors can be reduced by using a large number of Integral points per cell; however, this substantially increases the computational costs in the numerical integration.

Many efforts have been devoted to develop stable and efficient integration methods with reduced number of sampling points such as the nodal integration [14]-[16], the stress-point integration [17]-[18], the support domain integration [19].et al. Among these, the nodal integration initialed by Bessial and Belytschko [15] can dramatically improve the efficiency since it use the minimum evaluating points (the nodes) as integration points. However, direct nodal integration is not stable and can't pass the patch tests, lots of works have been done to relieve this issue. Among these, Chen *et al.* [20] developed a stabilized conforming nodal integration (SCNI) by using a strain smoothing method at the nodal representative domain, which is stable and provides even better accuracy than Gauss integration. It can pass the linear patch test whereas Gauss integration fails. One outstanding advantage of this method is that no additional term or stabilization parameter is involved. So far, SCNI has developed to be a major integration scheme in meshfree method and the strain smoothing technique in SCNI has been extend into FEM analysis [21].

This paper uses three-dimensional SCNI to simulate the temperature fields in single 316L stainless steel layers built on the substrate in SLM. The material properties are obtained from [7]. The remained of the paper is organized as follows. Section 2 presents a summary of the Mathematic model for SLM process. The stabilized conforming nodal integration (SCNI) and numeral examples are next presented in Section 3. Conclusions are then summarized in Section 4.

2. Mathematic model for selective laser melting (SLM) process

2.1 Thermal modelling

SLM is a swift remelting process. When the laser beam scans the surface of a powder bed, a portion of the laser energy is reflected and the remainder is absorbed by the powder. The absorbed laser energy melts the upper part of powder, thereby yielding a molten pool. Metallurgical bonds form between adjacent tracks and neighboring layers as solidification occurs.The thermal equilibrium equation satisfies the following classical 3D heat conduction equation [7]:

$$\rho c\frac{\partial T}{\partial t}=\frac{\partial}{\partial x}\left(k\frac{\partial T}{\partial x}\right)+\frac{\partial}{\partial \mathrm{y}}\left(k\frac{\partial T}{\partial y}\right)+\frac{\partial}{\partial \mathrm{z}}\left(k\frac{\partial T}{\partial z}\right)+Q \tag{1}$$

where ρ is the material density (kg/m^3); c is the specific heat capacity(J/kg K); T is the temperature; t is the interaction time; k is thermal conductivity (W/m K); and Q=(x, y, z, t) is the volumetric heat generation (W/m^3).
The effective thermal conductivity is a function of the powder's porosity [1]. The thermal conductivity of the powder can be expressed as [22],

$$k_p=k_b\left(1-\phi\right) \tag{2}$$

where ϕ is the porosity of the powder, it varies from 0.4 for powder state to 0 at solid state. k_p and k_b are thermal conductivities of powder and bulk materials.
Considering the melting and solidification phenomena that happen during additive manufacturing, the latent heat for phase change cannot be neglected. To define the latent heat of fusion, enthalpy is expressed as a function of temperature, T, density, p, and specific heat, c, according to

$$H=\int \rho c\left(T\right)dT \tag{3}$$

The material properties are obtained from [7]

2.1.1. Initial and boundary conditions

The initial temperature distribution throughout the powder bed at $t=0$ can be defined as

$$T\left(x,y,z,t\right)\big|_{t=0}=T_0,\quad \left(x,y,z\right)\in\Omega \tag{4}$$

where T_0 is the ambient temperature and is taken as 25 C.Since the layers are built on substrate with large thickness, the temperature at the bottom of the structure can be assumed to stay at T_0.

$$T\left(x,y,z,t\right)\big|_{z=0}=T_0 \tag{5}$$

During SLM, besides thermal conduction, heat losses due to convection should also be taken into account for proper description of the thermal behavior.The natural boundary condition can be expressed as [23]

$$k\frac{\partial T}{\partial n}+q_c=0,\quad \left(x,y,z\right)\in\Gamma_c \tag{6}$$

where Γ_c represents the surfaces attached to imposed heat fluxes(convection), n is the normal vector of Γ_c, and q_c is heat convection defined as

$$q_c = h\left(T - T_0\right) \tag{7}$$

where h is the coefficient for heat convection.

2.1.2. Heat source model

Heat input model: The Gaussian cylindrical source heat input model is used to simulate the heat input on to the part. The heat source distribution Q is given by

$$Q = \frac{AP}{\pi r_0^2 h} \exp\left(-\frac{r^2}{r_0^2}\right) \tag{8}$$

r is the distance from the laser center to the point, r_0 is the laser beam waist radius, P is the laser power, A is the absorptivity of the powder material which can be calculated if the reflectivity of the material k is known. (a reflectivity of iron=0.7 is considered for 316L stainless steel).

3. Numerical solution: meshfree method with stabilized conforming nodal integration (SCNI)

3.1 meshfree method

EFG uses the moving-least squares (MLS) approximation to construct the nodal shape functions. Given a set of nodes $\mathbf{X}_I$ in the domain $\Omega \subset \mathbf{R}^3$, the MLS approximation of the displacement is

$$\mathbf{u}^h(\mathbf{x}) = \mathbf{N}(\mathbf{x})\mathbf{U} = \sum_I \mathbf{N}_I(\mathbf{x})\mathbf{U}_I \tag{9}$$

where $\mathbf{U}$ is the vector of nodal displacement parameters. $\mathbf{N}(\mathbf{x})$ is the matrix of nodal shape functions which can be written as

$$N_I(\mathbf{x}) = \mathbf{p}^{\mathrm{T}}(\mathbf{X}_I) w_I(\mathbf{x}) \boldsymbol{\alpha}(\mathbf{x}) \tag{10}$$

where $\mathbf{p}(\mathbf{x})$ is a vector of base functions which usually includes a complete basis of the polynomials to a given order, $w_I(\mathbf{x})$ a weight function and $\boldsymbol{\alpha}(\mathbf{x})$ the unknown vector. The unknown vector $\boldsymbol{\alpha}(\mathbf{x})$ can be determined by the so called reproducibility condition, i.e. the consistency condition

$$\mathbf{p}(\mathbf{x}) = \sum_I \mathbf{p}(\mathbf{X}_I) N_I(\mathbf{x}) \tag{11}$$

Substitution of Eq.(10) into Eq.(11) leads to

$$\mathbf{A}(\mathbf{x})\boldsymbol{\alpha}(\mathbf{x}) = \mathbf{p}(\mathbf{x}) \tag{12}$$

where

$$\mathbf{A}(\mathbf{x}) = \sum_I \mathbf{p}(\mathbf{X}_I)\mathbf{p}^{\mathrm{T}}(\mathbf{X}_I) w_I(\mathbf{x}) \tag{13}$$

The nodal MLS shape functions $N_I(\mathbf{x})$ can be obtained from Eq.(11) after the unknown vector $\boldsymbol{\alpha}(\mathbf{x})$ is solved from Eq.(12). Computation of the derivatives of the MLS shape functions is by taking the derivative of Eq.(10)

$$N_{I,i}(\mathbf{x}) = \mathbf{p}^{\mathrm{T}}(\mathbf{X}_I)\left[w_{I,i}(\mathbf{x})\boldsymbol{\alpha}(\mathbf{x}) + w_I(\mathbf{x})\boldsymbol{\alpha}_{,i}(\mathbf{x})\right] \tag{14}$$

where subscripts preceded by commas denote partial derivatives with respect to spatial coordinates. The unknown $\boldsymbol{\alpha}_{,i}(\mathbf{x})$ in Eq.(7) can be solved from the derivative of Eq.(13)

$$\mathbf{A}(\mathbf{x})\boldsymbol{\alpha}_{,i}(\mathbf{x}) = \mathbf{p}_{,i}(\mathbf{x}) - \mathbf{A}_{,i}(\mathbf{x})\boldsymbol{\alpha}(\mathbf{x}) \tag{15}$$

with

$$\mathbf{A}_{,i}(\mathbf{x}) = \sum_I \mathbf{p}(\mathbf{X}_I)\mathbf{p}^{\mathrm{T}}(\mathbf{X}_I)w_{I,i}(\mathbf{x}) \tag{16}$$

3.2 Consistent integration schemes

In order to develop a stabilized nodal integration for the Galerkin meshfree method to achieve higher efficiency with desired accuracy and convergent properties, Chen *et al.* [20] developed a stabilized conforming nodal integration (SCNI). The Strain smoothing method used in SCNI at the nodal representative domain depends on

$$\tilde{u}^h_{,i}(\mathbf{X}_L) = \frac{1}{A_L}\int_{\Omega_L} u^h_{,i}\, d\Omega, \quad A_L = \int_{\Omega_L} d\Omega \tag{17}$$

where Ω_L is a nodal representative domain-the yellow cube covered by the Γ_L in Figure 2(a). Applying divergence theorem to Equation (17), the smoothed gradient operator can be rewritten as

$$\tilde{u}^h_{,i}(\mathbf{X}_L) = \frac{1}{A_L}\int_{\Gamma_L} \mathbf{n}u^h_i\, d\Gamma \tag{18}$$

where Γ_L is the boundary of the representative domain as shown in Figure 2. Introducing MLS shape functions into (17) yields

$$\tilde{N}_{I,i}(\mathbf{X}_L) = \frac{1}{A_L}\int_{\Gamma_L} \mathbf{n}N_{I,i}\, d\Gamma \tag{19}$$

The discrete form of (19) is

$$\tilde{N}_{I,i}(\mathbf{X}_L) = \frac{1}{A_L}\int_{\Gamma_L} \mathbf{n}N_{I,i}\, d\Gamma = \frac{1}{A_L}\sum_{L=1}^{NS}\sum_{G=1}^{NG} N_I(\mathbf{X}_L)n^L_i w_G \tag{20}$$

where *NS* is the number of the sides of the representative domain, *NG* the number of the gauss points per side. n^L_i the unit normal vector of the boundary. w_G the weight of the gauss points.

The whole computational domain is partitioned by background eight-node hexahedral element and each element represents an integration sub-domain (cell), as shown in Figure 2(a). The purple star is not only approximation node but cubature point, thus it is a one-point node integration scheme. The blue ridges denote the edge of background integration mesh. The four red crosses on each surface of the hexahedral cell are the quadrature points for boundary integration.

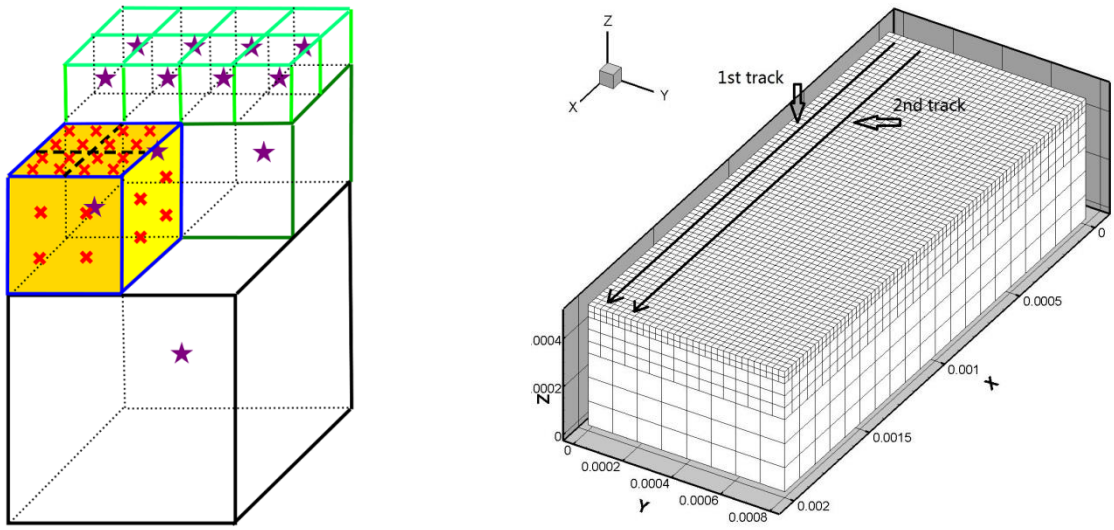

(a) (b)

Figure 2. (a) Schematic diagram of integration schemes for SCNI. (b) Three dimensional model of SLM.

3.3 Numerical example 1

In this paper, we constructed a self-adaption coarsening model as shown in Figure 2(b) .The size of it is $2.0mm \times 0.8mm \times 0.5mm$. The upper part of the structure is divided into fine mesh. All the topmost elements are given the powder's thermophysical parameter at first. If the laser scans on the element, it will be activated in the post process, and thermophysical parameter will change. When the heat affected zone moved away from the elements, a grid coarsening operation will be done to accelerate computing. The Table 1 presents the parameters in SLM:

Table 1. Parameters for SCNI simulation

Parameter	Value
Powder layer thickness, d	0.025mm
Laser spot size, D	0.1mm
Hatch spacing, s	0.0mm
Laser power, P	100,150,200W
Scan speed, v	50,100,200mm/s

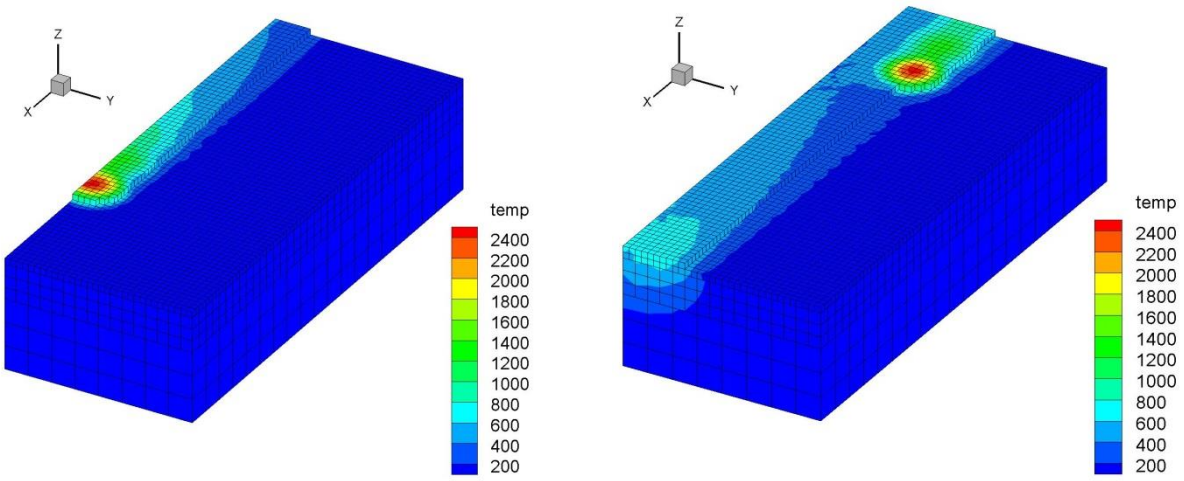

(a) (b)

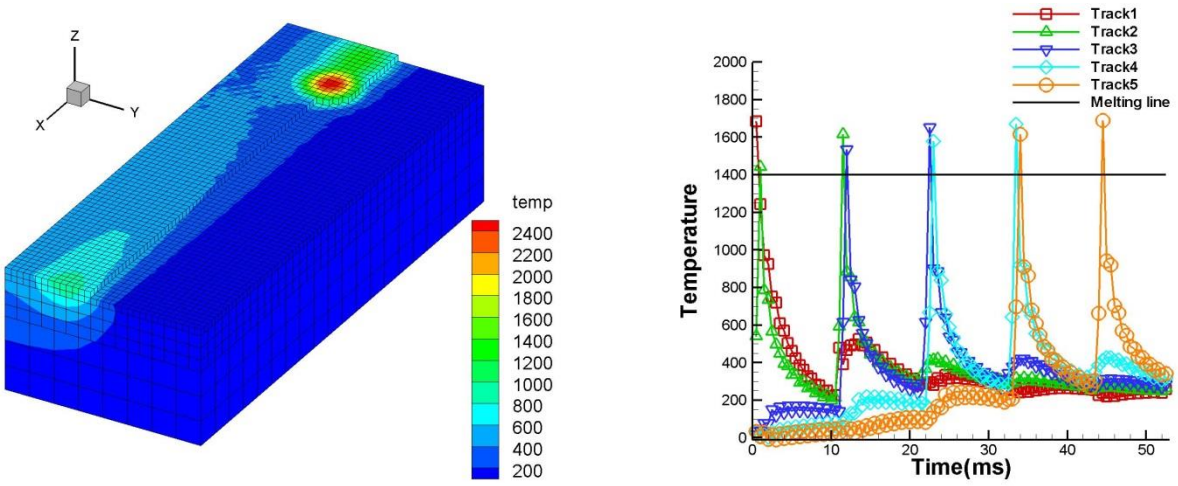

(c) (d)

Figure 3. (a) Temperature distribution at 1st track in the 20's layer. (b) Temperature distribution at 2nd track in the 20's layer. (c) Temperature distribution at 3rd track in the 20's layer. (d) Temperature history of the points in different track.

Figure 3 (a)-(c) show the temperature distribution as the laser beam reaches different positions during SLM for a scan speed of 100 mm/s and laser power of 150 W. When the first track was irradiated, the predicted maximum temperature of the powder bed was 2546 C in the region under direct irradiation, exceeding the melting point of 316L stainless steel powder(1398 C). The minimum temperature is only 25 C in the majority of the area of the substrate, At the beginning of the 2ed scan track, the maximum temperature of the structure soars to 2620 C. At the 3rd scan track, it increases to 2638 C. From the Figure 3 (d), we can also get the conclusion above. Every track melts twice during the scan, and after the 5th scan, almost the whole surface's temperature increases to 200 C.

3.4 Numerical example 2

We use another model to study the scan speed and power's affect on the molten pool, the physical dimension is $0.8mm \times 0.5mm \times 1.0mm$, other parameters are the same as example1.

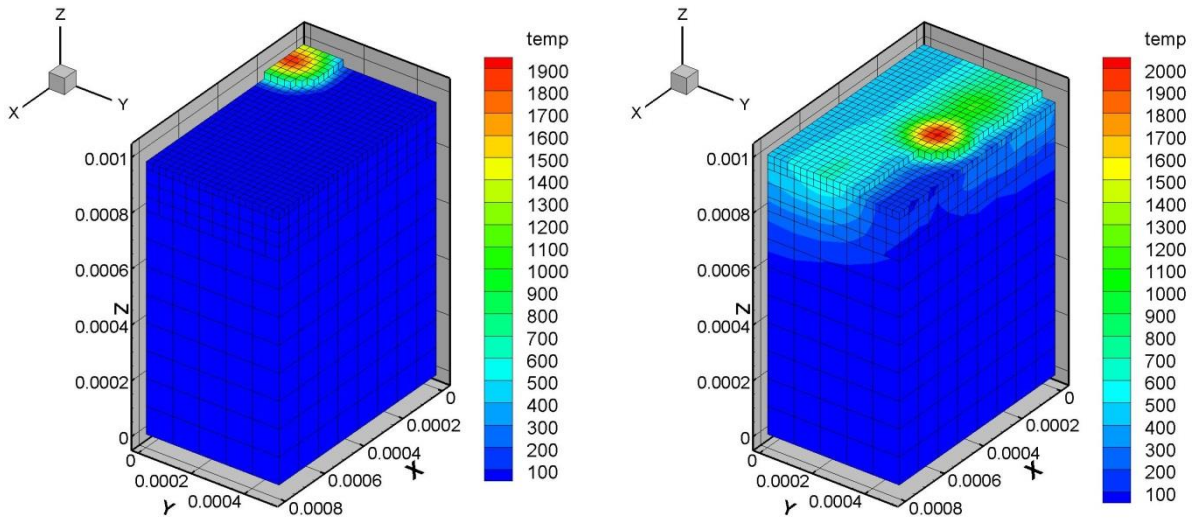

(a) (b)

Figure 4. (a) Scanning 1st track in the 40th layer. (b) Scanning 3rd track in the 40th layer.

Figure 4 (a)(b) demonstrate the temperature distribution when the laser beam reaches different track in manufacturing.

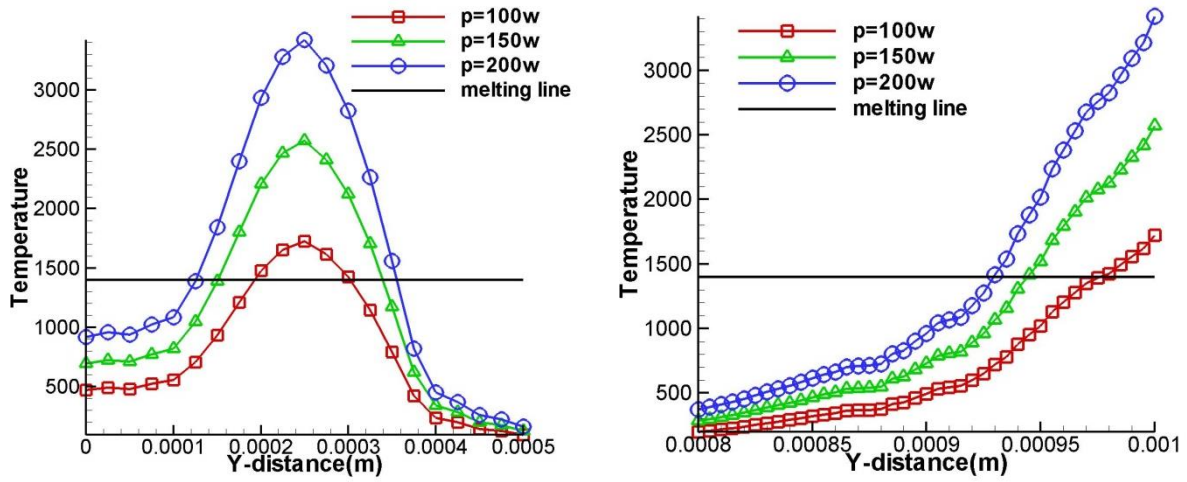

(a) (b)

Figure 5. (a) Distribution of temperature along Y-axis at the molten pool of 3rd layer for different laser power. (b) Distribution of temperature along Z-axis at the molten pool of 3rd layer for different laser power.

Figure 5 exhibits the molten pool size for a given scan speed of 100mm/s as the laser power changes. If the laser power is 100W, the width and the depth are only 0.1mm and 0.025mm. When the laser power changes to 200W the width and the depth observably increase to 0.23mm and 0.072mm, respectively. It indicates that laser power has a significant influence on the molten pool.

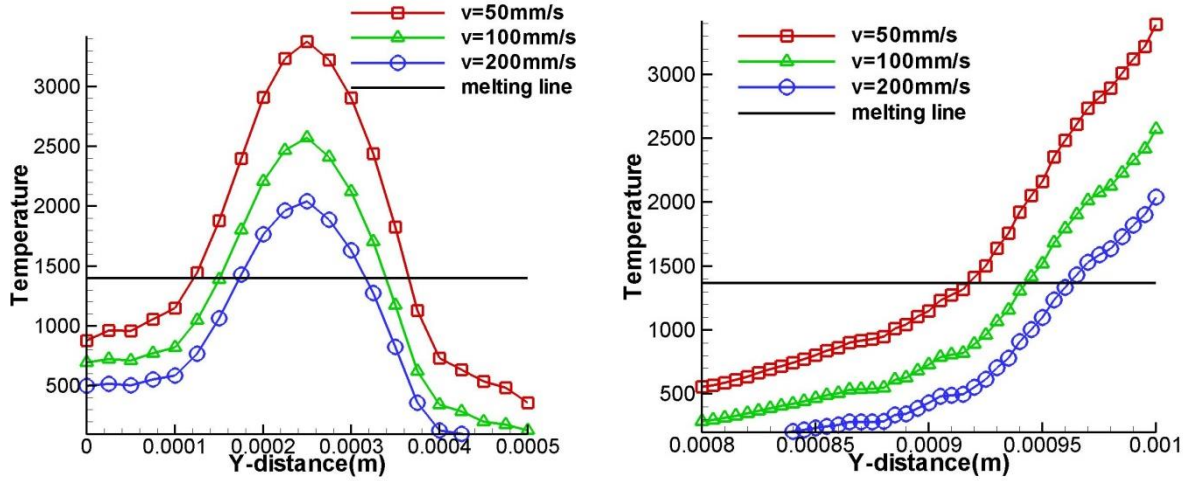

(a) (b)

Figure 6. (a) Distribution of temperature along Y-axis at the molten pool of 3rd layer for different scan speed. (b) Distribution of temperature along Z-axis at the molten pool of 3rd layer for different scan speed.

Figure 6 shows the width and depth of molten pool for a given laser power of 150W, when the scan speed changes from 50mm/s to 200mm/s. The width and the depth are 0.15mm and 0.035mm, since the scan speed is 200mm/s. When the scan speed decreases to 50mm/s, the width and the depth markedly increase to 0.24mm and 0.073mm. Just like the laser power, Scan speed impacts the pool size obviously.

4. Conclusion

Three dimensional meshfree method is developed for predicting the temperature fields within a single metallic layer formed on the substrate in SLM process. The major findings are:

1. The proposed meshfree method is able to simulate the heat transfer in SLM.
2. Due to heat accumulation, the maximum and average temperatures gradually increase during the SLM process. And this is demonstrated in this paper.
3. Both the scan speed and power have impact on the molten pool and its size can be predicted by the developed method.

5. Acknowledgement

The authors are pleased to acknowledge the support of this work by Science Challenge Project (No. JCKY2016212A502), the National Key Research and Development Program of China (2016YFC1402705, 2016YFC1402706), the National Natural Science Foundation of China (11372066, 11232003), the Fundamental Research Funds for the Central Universities(DUT15LK07), the open funds of the state key laboratory of water resources and hydropower engineering science (2015SGG03), the open funds of the state key laboratory of Geohazard Prevention and Geoenvironment Protection (SKLGP2016K007).

References

[1] Kruth JP, Levy G, Klocke F, Child THC. (2007) Consolidation phenomena in laser and powder-bed based layered manufacturing, *CIRP Ann Manuf Technol* **56**, 730–59.
[2] Gu DD, Meiners W, Wissenbach K, Poprawe R. (2012) Laser additive manufacturing of metallic components: materials, processes and mechanisms. *IntMater Rev* **57**, 133–64.
[3] Gusarov AV, Yadroitsev I, Bertrand P, Smurov I. (2007) Heat transfer modelling and stability analysis of selective laser melting, *Appl Surf Sci* **254**, 975–9.
[4] Gusarov AV, Smurov I. (2009) Two-dimensional numerical modelling of radiation transfer in powder beds at selective laser melting, *Appl Surf Sci* **255**, 5595-5509.
[5] Gusarov AV, Smurov I. (2010) Modeling the interaction of laser radiation with powder bed at selective laser melting, *Phys Proc* **5**, 381–94.
[6] Y. Li, D. Gu. (2014) Thermal behavior during selective laser melting of commercially pure titanium powder: numerical simulation and experimental study, *Addit. Manuf.* **1**, 99–109.
[7] A. Hussein, L. Hao, C. Yan, R. Everson, (2013) Finite element simulation of the temperature and stress fields in single layers built without-support inselective laser melting, *Mater. Des.* **52**, 638–647.
[8] Nayroles B, Touzot G, Villon P. (1992) Generalizing the finite element methods: Diffuse approximation and diffuse elements, *Computational Mechanics* **10**, 307-318.
[9] Belytschko T, Lu YY, Gu L. (1994) Element-free Galerkin methods, *International Journal for Numerical Methods in Engineering* **37**, 229–256.
[10] Liu W.K., Jun S, Zhang Y.F. (1994) Reproducing kernel particle methods, *International Journal for Numerical Methods in Fluids* **20**, 1081–1106.
[11] Duarte CA, Oden JT. (1996) H-p clouds—an h-p meshless method, *Numer. Methods Partial Differ. Equations* **12**, 673-705.
[12] Zhang X. (2001) Least-Squares collocation meshless method, *International Journal for Numerical Methods in Engineering* **51**, 1089–1100.
[13] Liu GR, Gu YT and Dai K. (2004) Assessment and applications of point interpolation methods for computational mechanics, *International Journal for Numerical Methods in Engineering* 59, 1373-1397.
[14] Dolbow J, Belytschko T. (1999) Numerical integration of the Galerkin weak form in meshfree methods, *Computational Mechanics* **23**, 219–230.
[15] Beissel S, Belytschko T. (1996) Nodal integration of the element-free Galerkin method, *Computer Methods in Applied Mechanics and Engineering* **139**, 49–74.
[16] Liu GR, Zhang GY, Wang YY, Zhong ZH, Li GY, Han X. (2007) A nodal integration technique for meshfree radial point interpolation method (NI-RPIM) , *International Journal of Solids and Structures* **44**, 3840–3860.
[17] Dyka CT, Randles PW, Ingel RP. (1997) Stress points for tension instability in SPH, *International Journal for Numerical Methods in Engineering* **40**, 2325–2341.
[18] Fries TP, Belytschko T. (2008) Convergence and stabilization of stress-point integration in mesh-free and particle methods, *International Journal for Numerical Methods in Engineering* **74**, 1067–1087.

[19] Liu Y, Belytschko T. (2010) A new support integration scheme for the weak form in mesh-free methods, *International Journal for Numerical Methods in Engineering* **82**, 699–725.
[20] Chen JS, Wu CT, Yoon S, You Y. (2001) A stabilized conforming nodal integration for Galerkin mesh-free methods, *International Journal for Numerical Methods in Engineering* **50**, 435–466.
[21] Liu G, Dai K, Nguyen T. (2007) A smoothed finite element method for mechanics problems, *Computational Mechanics* **39**, 859-877.
[22] Thummler F, Oberacker R. (1993) An introduction to powder metallurgy, Cambridge (London): The University Press.
[23] Dai K, Shaw L. (2005) Finite element analysis of the effect of volume shrinkage during laser densification, *Acta Mater* **53**, 4743–54.